A transmission electron microscopy study of low-strain epitaxial $BaTiO_3$ grown onto $NdScO_3$

T Denneulin[1,2] and A S Everhardt[3]

[1]Ernst Ruska Centre for Microscopy and Spectroscopy with Electrons and Peter Grünberg Institute, Forschungszentrum Jülich, Jülich 52425, Germany

[2]CEMES, CNRS, 29 rue Jeanne Marvig, 31055 Toulouse, France

[3]Zernike Institute for Advanced Materials, University of Groningen, 9747 AG Groningen, The Netherlands

E-mail: t.denneulin@fz-juelich.de

Abstract. Ferroelectric materials exhibit a strong coupling between strain and electrical polarization. In epitaxial thin films, the strain induced by the substrate can be used to tune the domain structure. Substrates of rare-earth scandates are sometimes selected for the growth of ferroelectric oxides because of their close lattice match, which allows the growth of low-strain dislocation-free layers. Transmission electron microscopy (TEM) is a frequently used technique for investigating ferroelectric domains at the nanometer-scale. However, it requires to thin the specimen down to electron transparency, which can modify the strain and the electrostatic boundary conditions. Here, we have investigated a 320 nm thick epitaxial layer of $BaTiO_3$ grown onto an orthorhombic substrate of $NdScO_3$ with interfacial lattice strains of -0.45% and -0.05% along the two in-plane directions. We show that the domain structure of the layer can be significantly altered by TEM sample preparation depending on the orientation and the geometry of the lamella. In the as-grown state, the sample shows an anisotropic a/c ferroelastic domain pattern in the direction of largest strain. If a TEM lamella is cut perpendicular to this direction so that strain is released, a new domain pattern is obtained, which consists of bundles of thin horizontal stripes parallel to the interfaces. These stripe domains correspond to a sheared crystalline structure (orthorhombic or monoclinic) with inclined polarization vectors and with at least four variants of polarization. The stripe domains are distributed in triangular-shaped 180° domains where the average polarization is parallel to the growth direction. The influence of external electric fields on this domain structure was investigated using *in-situ* biasing and dark-field imaging in TEM.

Keywords: Ferroelectrics, $BaTiO_3$, TEM, dark-field imaging, in-situ biasing

PACS numbers: 77.55.fe, 68.37.Lp, 61.05.jp

AMS classification scheme numbers:

Submitted to: *J. Phys.: Condens. Matter*

1. Introduction

Epitaxial thin layers of ferroelectric metal oxides have different applications in non-volatile memories [1] and micro-electro-mechanical systems (MEMS) [2]. The piezoelectric and ferroelectric properties of the layers are related to the nucleation and growth of nanoscale domains whose structure depends on multiple parameters such as the crystallography, the composition, the geometry, the mechanical and electrostatic boundary conditions. Domains can be classified as purely ferroelectric or ferroelastic depending on their sensitivity to an external stress. For instance, thin layers of tetragonal $Pb(Zr_xTi_{1-x})O_3$ can exhibit purely ferroelectric 180° domains, where the polarization is oriented in antiparallel directions [3–5]. Their role is to minimize depolarization fields induced by charges located at the interfaces, in the absence of sufficient screening charges (grounded electrodes). The layer can also contain 90° ferroelastic twin domains (*a/c* domains), where the polarization alternates between out-of-plane and in-plane directions [6–8]. These domains play a role in the relaxation of the interfacial strain induced by the epitaxial growth onto a lattice mismatched substrate [9, 10]. The ferroelastic domain structure can be tuned to some extent by strain engineering *i.e.* by choosing a substrate with an appropriate structure and lattice parameters with respect to those of the layer [11, 12].

Different techniques can be used to study ferroelectric domains such as optical microscopy [13], scanning electron microscopy (SEM) [14, 15], piezoresponse force microscopy (PFM) [16, 17] or X-ray diffraction [3, 18]. Transmission electron microscopy (TEM) allows the investigation of ferroelectric domains at the atomic-scale [19–21] and in the presence of external stimuli [22–24]. However, it requires to thin the material down to electron transparency (approximately 100 nm in thickness), which can modify the domain structure in different ways. First, elastic relaxation at the free surfaces of a TEM cross-section lamella is a long-known and inevitable problem [25, 26]. It modifies the strain fields in epitaxial samples and its significance depends on the thickness of the TEM slab with respect to the thickness of the layer. Second, ferroelectric domains have a tendency to shrink in size when the material is thinned down to the nanoscale. It has been reported that the size of 90° twin domains in single crystal $BaTiO_3$ depends significantly on the thickness of the TEM slab [27]. This phenomenon is usually associated to the law of Kittel, which states that the width of the domains is proportional to the square root of the thickness of the lamella [28]. This law was initially proposed for ferromagnetic samples but was later demonstrated for 180°

ferroelectric domains [29] and ferroelastic domains [9]. Third, the three-dimensional geometry of the sample also influences the domain structure. For instance, in nanowires of $BaTiO_3$ prepared by focused ion beam (FIB), the orientation of the 90° domains is influenced by depolarization fields, which are minimized when the non-axial polarization is perpendicular to the smallest surface [30, 31]. In nanodots of $BaTiO_3$, the domains form a quadrant field-closure arrangement and each quadrant is divided in 90° stripe domains [32]. Finally, a fourth problem in TEM is that ferroelectric oxides are electrical insulators and the accumulation of charges in the area illuminated by the electron beam produces an electric field, which can induce domain switchings [33–36]. On the one hand, these different phenomena can modify the domain structure with respect to the as-grown samples, which can be a problem if one wants to correlate the TEM observations to the bulk properties of the materials. On the other hand, these phenomena provide different pathways for the manipulation and the understanding of ferroelectric domains at the nanoscale.

Here, we have investigated an epitaxial layer of $BaTiO_3$ grown onto a [110]-oriented $NdScO_3$ substrate using TEM. $BaTiO_3$ is a classical lead-free ferroelectric with a particularly rich phase diagram [37, 38]. The closely-matched lattice of the $NdScO_3$ substrate provides a low strain, which avoids the formation of misfit dislocations and allow the stabilization of intermediate crystalline phases of low symmetry at room temperature [39, 40]. First, we have investigated the influence of TEM sample preparation on the ferroelectric and ferroelastic domain structure. Second, domain switching mechanisms in the presence of external fields have been studied *in-situ* TEM using a dedicated specimen holder equipped with an electrical microprobe.

2. Methods and conditions

The sample is a 320 nm thick $BaTiO_3$ layer with a 7 nm thick $SrRuO_3$ bottom electrode grown by pulsed layer deposition (PLD) onto a $[110]_{ortho}$-oriented orthorhombic substrate of $NdScO_3$ [39]. The deposition has been carried out using a Lambda Physik COMPex PRo 205 KrF ($\lambda = 248$ nm) excimer ultraviolet laser and a Twente Solid State Technology reflection high-energy electron diffraction (RHEED) vacuum system. The target was a $BaTiO_3$ single crystal (MaTecK GmbH) and the deposition parameters were a background pressure of 10^{-7} mbar, a substrate temperature of 700-800°C, a laser energy of 2 $J.cm^{-2}$, a spot size of 2.6 mm^2, a target-substrate distance of 50 mm, a repetition rate of 5 Hz and a P_{O_2} of 0.15 mbar. After the growth, the cooling rate was 5°C/min at 300 mbar P_{O_2}. The $NdScO_3$ substrate (CrysTec GmbH) was pre-treated to obtain single termination for 4 hours at 900°C in an oxygen flow and subsequently submerged in 12 M NaOH and 1 M NaOH for several hours followed by water/ethanol cleaning step.

Cross-section thin foils were prepared using a focused ion beam and a scanning electron microscope (FIB-SEM) FEI Helios platform. The surface of the sample was protected with three different layers of platinum. First, the surface was covered with a $\approx$ 100 nm thick Pt layer using physical vapor deposition (PVD) prior insertion into the FIB. Then, another $\approx$ 100 nm thick Pt layer was deposited locally using electron beam-induced deposition (EBID) and a $\approx$ 3 µm thick Pt layer was deposited on top using ion beam-induced deposition (IBID). The role of the two first layers is to prevent the implantation of ions in the $BaTiO_3$ layer during the third deposition step. 20×2×5 μm^3 pieces of samples were cut, lifted out from the bulk using a nanomanipulator, attached to a 3 mm copper grid using Pt IBID deposition and thinned to electron transparency. In the last steps of the thinning, the energy of the ion beam was decreased from 30 kV to 5 kV to minimize surface damage. Lamellas were prepared along the two perpendicular crystallographic directions of the substrate *i.e.* the $[001]_{ortho}$ and $[1\text{-}10]_{ortho}$ directions.

High resolution TEM (HRTEM) and scanning TEM with a high angle annular dark-field detector (HAADF STEM) were carried out using an FEI Titan TEM equipped with a 300 kV field emission gun, a CEOS image aberration corrector and a Gatan K2 4k×4k camera. Conventional dark-field TEM, dark-field electron holography and *in-situ* biasing were carried out using a Hitachi HF-3300 TEM equipped with a 300 kV cold field emission gun, a CEOS image aberration corrector, multiple electron biprisms and a Gatan OneView 4k×4k camera.

Conventional dark-field TEM imaging was used to image ferroelectric domains. The sample was oriented a few degrees out of zone-axis to enhance the intensity of a diffracted beam. The incident illumination was tilted to bring the diffracted beam onto the optical axis and a small objective aperture was used to isolate the diffracted beam. Under kinematic approximation, the Friedel's law states that the intensity of two opposite diffracted beams of reciprocal lattice vectors $\vec{g}$ and $-\vec{g}$ is equal ($I_g = I_{-g}$) even in non-centrosymmetric crystals. However, this law fails if the sample is sufficiently thick due to dynamical effects [41, 42]. By acquiring dark-field images with different diffracted beams, it is possible to identify the direction of the local polarization vector $\vec{P}$ as the dark-field contrast is related to the scalar product $\vec{g}.\vec{P}$ [43–45].

Dark-field off-axis electron holography was used to measure lattice deformations [46, 47]. The imaging conditions were similar to those used for dark-field imaging (see previous paragraph). An electron biprism was used to overlap the electron wave diffracted in the layer (object wave) with the wave diffracted in the substrate (reference wave). An elliptical illumination was formed using the condenser stigmators to improve the coherence in the direction perpendicular to the biprism. The fringe spacing was 2 nm and the hologram width was 400 nm. Phase images were reconstructed from the holograms using Fourier transform operations in the Digital Micrograph software (Gatan). Lattice deformation and rotation maps were calculated from the gradient of the phase in the directions parallel and perpendicular to the selected $\vec{g}$ vector, respectively. Deformations and rotations are defined in percentages and degrees with respect to the substrate's lattice. The spatial resolution in the reconstructed maps is 8 nm (determined by the size of the aperture in Fourier space).

Ferroelectric domain switching in the presence of external electric fields was investigated using a Hysitron PI 95 Picoindenter TEM holder equipped with a B-doped (10^{21} cm^{-3}) cube-corner-shaped diamond probe. The probe was moved inside the microscope using micrometer screws for the coarse motion and piezoelectric motors for the final approach until a contact was established with the Pt capping layer of the TEM lamella (acting as a top electrode). The nanoECR mode (nanoscale Electrical Contact Resistance) was used to apply different voltages up to $\pm$40 V. Videos were recorded using the HD video module of the Digital Micrograph software (Gatan) with a frame rate of 5 images per second and an image size of approximately 800$\times$800 pixels. The speed of the videos provided in Supplementary Materials was increased several times to reduce the size of the files.

3. Results

3.1. Description of the crystalline and ferroelectric domain structures

Fig. 1(a) is an overview Z-contrast HAADF STEM image of the sample, which shows a uniform contrast inside the $BaTiO_3$ layer. The crystalline quality of the interfaces was investigated using HRTEM. Fig. 1(b,c) shows HRTEM images of the $BaTiO_3/SrRuO_3/NdScO_3$ bottom interfaces, in two different lamellas cut parallel to the two in-plane directions $[001]_{ortho}$ and $[1\text{-}10]_{ortho}$, respectively. The insets in the top-right corners are the corresponding Fourier transforms, which show sharp and regularly spaced peaks. In

$NdScO_3$ (orthorhombic)	a_{NdScO_3} 0.5575 nm	b_{NdScO_3} 0.5776 nm	c_{NdScO_3} 0.8003 nm
	$d^{(110)}_{NdScO_3}$ 0.4014 nm		$d^{(002)}_{NdScO_3}$ 0.4002 nm
$BaTiO_3$	$a^{cubic}_{BaTiO_3}$ 0.4000 nm	$a^{tetra}_{BaTiO_3}$ 0.3992 nm	$c^{tetra}_{BaTiO_3}$ 0.4036 nm
$(a_{BaTiO_3} - d^{(002)}_{NdScO_3})/d^{(002)}_{NdScO_3}$	-0.05%	-0.25%	+0.85%
$(a_{BaTiO_3} - d^{(110)}_{NdScO_3})/d^{(110)}_{NdScO_3}$	-0.45%	-0.55%	+0.55%

Table 1. From top to bottom: Bulk lattice parameters of orthorhombic $NdScO_3$ [48] as well as (110) and (002) d-spacings corresponding to the lattice parameters of a primitive perovskite unit cell ((001) and (100) d-spacings). Bulk lattice parameters of cubic and tetragonal $BaTiO_3$ [49, 50]. Corresponding lattice mismatches between $NdScO_3$ and $BaTiO_3$.

both directions, the crystalline quality and the epitaxial alignment of the lattices of the layers and the substrate were found to be excellent. No misfit dislocations were observed at the interfaces.

In the absence of stress, $BaTiO_3$ is expected to be tetragonal at room temperature and cubic at the growth temperature (the Curie temperature being $T_c \approx 120°C$). In order to understand the lattice match between the substrate and the layer, the theoretical lattice parameters of orthorhombic $NdScO_3$, cubic and tetragonal $BaTiO_3$ are indicated in Table 1. The corresponding values of lattice strain in the two orthogonal in-plane directions are also indicated. For cubic $BaTiO_3$, there is nearly no strain (-0.05%) in the $[001]_{ortho}$ direction and there is a small tensile strain (-0.45%) in the $[1\text{-}10]_{ortho}$ direction. For tetragonal $BaTiO_3$, if the a-axis is assumed to be in-plane, it leads to slightly larger tensile strains (respectively -0.25% and -0.55%). If the c-axis is in-plane, it leads to compressive strains (respectively +0.85% and +0.55%). Therefore, at room temperature, the c-axis could be oriented either out-of-plane or in-plane along the $[1\text{-}10]_{ortho}$ direction, but probably not along the $[001]_{ortho}$ direction to avoid large strains. This description is valid for the as-grown bulk sample. After thinning, the strain should be maintained along the direction that is parallel to the lamella and to the interface, but it could be partially relaxed along the electron beam direction.

In order to investigate the ferroelectric domain structure, dark-field TEM images were acquired using two different diffracted beams associated to $\overrightarrow{g}$ vectors that are perpendicular or parallel to the interfaces. Fig. 2(a,b) show $(220)_{ortho}$ and $(004)_{ortho}$ dark-field images

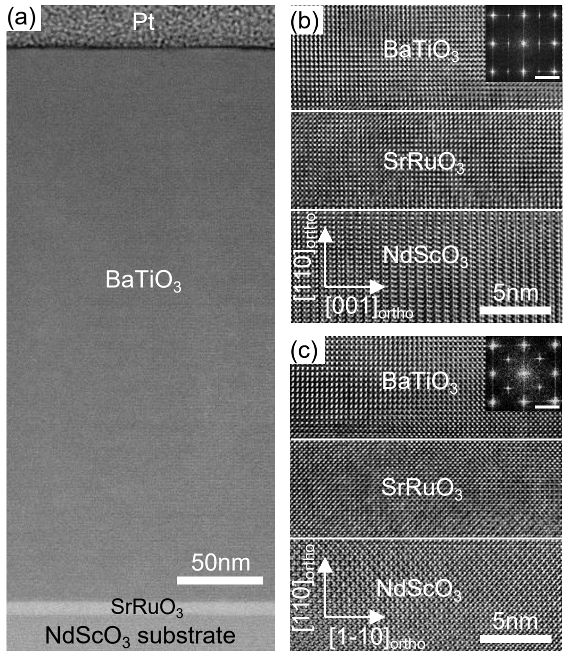

Figure 1. (a) HAADF STEM image of the 320 nm $BaTiO_3$ layer with a 7 nm thick $SrRuO_3$ bottom electrode grown onto a [110]-oriented $NdScO_3$ substrate. (b,c) HRTEM images of the $NdScO_3/SrRuO_3/BaTiO_3$ interfaces in two different lamellas cut parallel to the $[001]_{ortho}$ and $[1\text{-}10]_{ortho}$ crystallographic directions of the substrate, respectively. The insets in the top-right corner are the corresponding Fourier transforms (scale bar is 2 nm^{-1}).

obtained in the lamella cut parallel to the $[001]_{ortho}$ direction, where the contrast is related to the vertical and horizontal components of the ferroelectric polarization, respectively. In (a), triangular-shaped domains with a bright contrast are visible in the top part of the $BaTiO_3$ layer. They most likely correspond to 180° domains with vertical polarization vectors (either up or down) and whose triangular shape reduces the density of charges at the domain walls [51]. They are not visible in (b) because the polarization has no horizontal component in these domains. Fig. 2(c) shows a simplified schematic of the ferroelectric domain structure where the direction of the polarization vectors is indicated with arrows.

Fig. 2(d,e) show the corresponding vertical $(220)_{ortho}$ and horizontal $(2\text{-}20)_{ortho}$ dark-field images obtained in the lamella cut parallel to the $[1\text{-}10]_{ortho}$ direction. Again, triangular-shaped 180° domains are visible in (d), in the top part of the $BaTiO_3$ layer. However the triangular shape of the domains is slightly different as they are roughly isosceles in (a) and rectangle in (d). This difference is related to the presence of 90° domains (or a/c twins) with domain walls at 45° to the interfaces (parallel to the <110> planes of the $BaTiO_3$). These twin domains can be seen in both (d and e) because the polarization alternates between

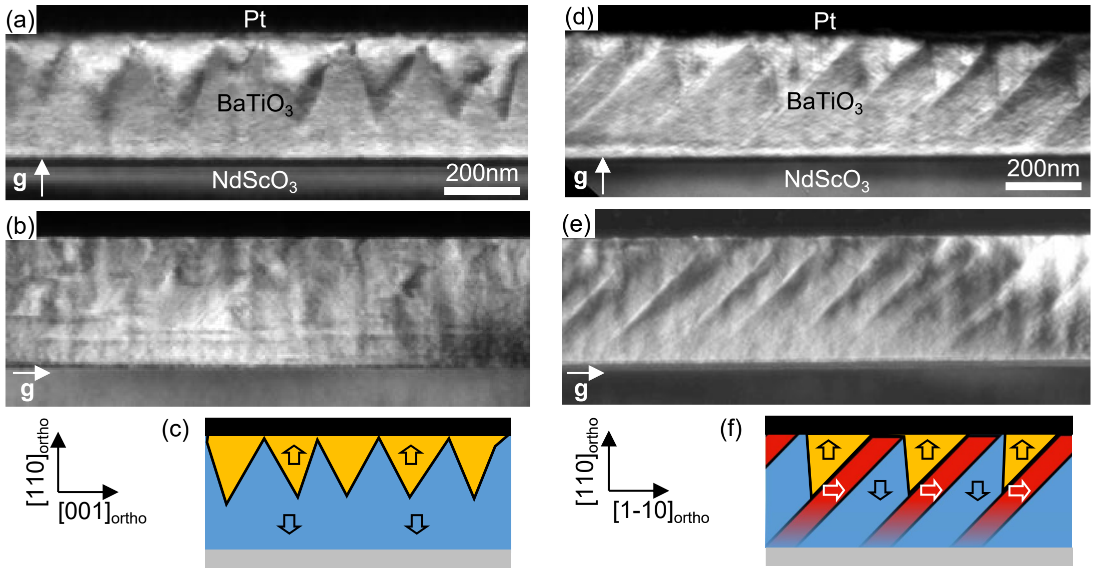

Figure 2. (a) Vertical $(220)_{\mathrm{ortho}}$ and (b) horizontal $(004)_{\mathrm{ortho}}$ dark-field images of a cross-section lamella cut along the $[001]_{\mathrm{ortho}}$ direction. The contrast is related respectively to the vertical and horizontal components of the polarization. (c) Corresponding schematic of the ferroelectric domain structure and polarization directions (the sign of the indicated polarization vectors was not determined and could be the opposite). (d) Vertical $(220)_{\mathrm{ortho}}$ and (e) horizontal $(2\text{-}20)_{\mathrm{ortho}}$ dark-field images in a cross-section lamella cut along the $[1\text{-}10]_{\mathrm{ortho}}$ direction. (f) Corresponding schematic of the ferroelectric domain structure.

vertical and horizontal directions in the image plane. Fig. 2(f) is the corresponding schematic of the domain structure. The 90° domains form an obstacle for the 180° domains and the a/c boundaries can become charged because of the tail-to-tail or head-to-head configuration of the polarization at the domain walls (interactions between 90° and 180° domains have been described in [22, 23]). The contrast of the a/c domains appears gradually along the growth direction because the tetragonality increases as the epitaxial strain is relaxed away from the bottom interface. Lattice deformation measurements, shown in Supplementary Information 1 and in Ref. [40], confirm the progressive increase of the tetragonality along the vertical direction.

In summary, the $BaTiO_3$ layer shows purely ferroelectric 180° domains in both perpendicular cross-section lamellas. The zig-zag 180° domain walls are located primarily in the top part of the film and so the bottom domain covers a larger area in the image compared to the top domains. a/c twin domains are visible only in one of the two perpendicular cross-sections, which indicates that the ferroelastic domain pattern is anisotropic. This is also confirmed by a PFM image of the surface of the sample shown in Supplementary

Information 2. This anisotropy is related to the orthorhombic structure of the substrate and the fact that the strain is slightly different in the $[1\text{-}10]_{ortho}$ direction and the $[001]_{ortho}$ direction. It is difficult to determine if the a/c domains observed in Fig. 2(d,e) exist in the TEM sample of Fig. 2(a,b) because the domain walls would then be inclined at 45° to the electron beam direction and may not produce sharp variations of contrast. However, because of the absence of crystallographic defects to pin the a/c domains and because of a possible strain relaxation at the free surfaces of the lamella, the ferroelastic domain pattern could also be altered in this geometry. In order to obtain more information about the influence of the lamella geometry on the domain structure, a TEM lamella with varying thickness was prepared.

3.2. Influence of the thickness and the geometry of the TEM lamella on the ferroelectric domain structure

Fig. 3(a) shows a low magnification TEM image of a staircase-shaped lamella with different thicknesses, which was cut parallel to the $[001]_{ortho}$ direction (same cut as in Fig. 2(a-c)). The thickness of the lamella along the electron beam direction was measured by SEM and is approximately 140, 110 and 80 nm (±20 nm) in the three different regions. The thickness of the Pt capping decreases with the thickness of the lamella. Part of the capping was inevitably milled away when the lamella was thinned down because of the Gaussian shape of the incident ion beam [52]. Fig. 3(b-d) shows vertical $(220)_{ortho}$ dark-field images acquired in the three different regions, which exhibit a continuous distribution of triangular-shaped 180° domains in the top part of the layer. The size of the domains decreases with the thickness of the lamella as they are approximately four times smaller in (d) than in (b). As a consequence, the bottom apex of the triangular domains is located near the middle of the film in (b) and closer to the top electrode in (d). It can also be noticed in (b-d) that the contrast is brighter in the bottom part of the $BaTiO_3$ layer, over a distance of ≈ 50 nm to the interface with the $SrRuO_3$. This could be attributed to strain relaxation at the free surfaces of the lamella, which leads to a bending of the horizontal lattice planes along the electron beam direction and thus to local variations of the dark-field intensity close to the interface. Fig. 3(e-g) show the corresponding $(004)_{ortho}$ horizontal dark-field images. Interestingly, narrow horizontal domains can be noticed in (g), as indicated by arrows in the image. These domains are 10 to 20 nm large in the vertical direction and a few hundreds of nanometers long in the horizontal direction. On close inspection, it seems possible that such horizontal domains also exist in (e,f), but with lower contrast.

The decrease in size of the 180° domains could be related to the thickness of the TEM lamella and/or the thickness of top Pt electrode. Previous studies have reported that the periodicity of 180° domains decreases with the thickness of the crystal [3, 53]. Other studies have reported that the thickness of the top electrode can influence the ferroelectric imprint (horizontal shift of the hysteresis curve) and so modify the polar ground state [40, 54]. The presence of horizontal stripes is quite unusual in titanate thin films. In first impression, they could be attributed to tetragonal 90° domains with domain walls at 45° to the electron beam direction, as observed in Ref. [30]. Previously, such domains were observed in nanowires of $BaTiO_3$, in which the non-axial polarization is perpendicular to the smallest surface of the wire to minimize depolarization fields. However, in the case of a lamella, the polarization should rather stay in the plane of the lamella to minimize depolarization fields and should not point directly towards the free surfaces. In addition, such 90° domains would be visible in the vertical dark-field images and not in the horizontal images, which is the opposite to what is observed here. Since the domains are only visible in the horizontal dark-field images, it can be deduced that there is only a change of the horizontal component of the polarization.

A more detailed analysis of these stripe domains is shown in Fig. 4. Previously, thick regions of sample were left on the sides of the lamella. Here, the lamella was also cut on the left and right sides as indicated by arrows in the horizontal $(004)_{\mathrm{ortho}}$ dark-field image in Fig. 4(a). The top and bottom electrodes are then disconnected from the grounded Cu grid and only the insulating $NdScO_3$ substrate remains connected to the grid. These additional cuts are made to avoid current leakage in later electrical biasing experiments. However, these cuts also change the electrical and mechanical boundary conditions, which can in turn modify the domain structure. Fig. 4(b) is a magnified image of the $BaTiO_3$ layer, which shows horizontal stripes with alternating bright/dark contrast, similar to those observed in Fig. 3(g) but with a larger density. The region indicated by a dashed rectangle in Fig. 4(b) is further magnified in Fig. 4(c). The presence of a triangular-shaped 180° domain is indicated by a red solid curve and a bundle of horizontal stripe domains is indicated with red dashed horizontal lines. It can be observed that the contrast of the horizontal stripes is inverted when they cross the 180° domain wall as the bright stripes become dark and *vice versa*. Strain measurements were carried out to obtain more information on the crystalline structure of these stripes. Fig. 4(d,e,f,g) show a $(004)_{\mathrm{ortho}}$ dark-field electron hologram, the reconstructed ε_{xx} horizontal deformation map, the ω_{xy} rotation map, and profiles extracted from the maps

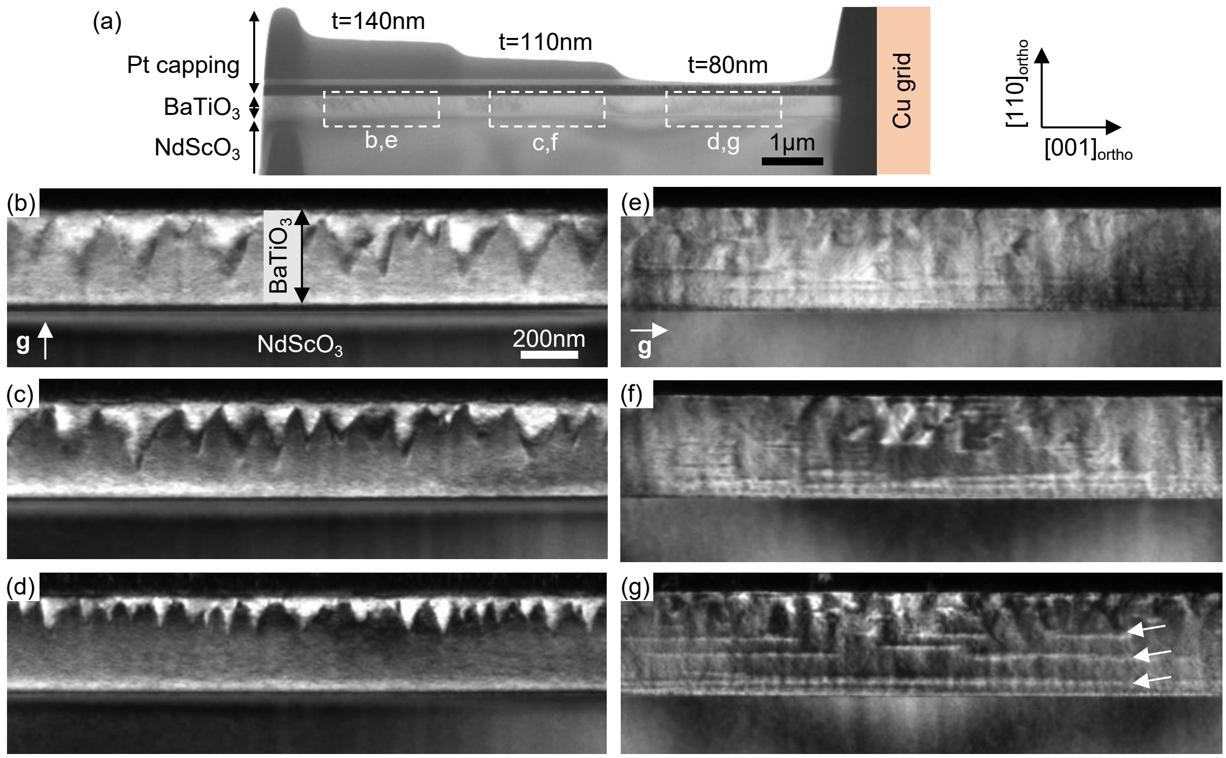

Figure 3. (a) Low magnification TEM image of a staircase-shaped lamella with three distinct regions of 2 to 3 µm large and different thicknesses (t = 140 nm, 110 nm and 80 nm) cut parallel to the $[001]_{ortho}$ direction. (b,c,d) Vertical $(220)_{ortho}$ and (e,f,g) horizontal $(004)_{ortho}$ dark-field TEM images obtained in the three different regions as indicated by dashed rectangles in (a). The contrast is related respectively to the vertical and horizontal components of the polarization.

along the growth direction, respectively. No significant deformation was observed in the stripes but an alternating positive and negative tilt of the vertical planes of at most $\pm 0.1°$ was measured.

Based on the previous observations, a schematic of the domain structure is proposed in Fig. 4(h) where the angles have been purposely exaggerated. The stripes are associated to a tilt of the polarization vectors with respect to the vertical direction, which is related to a shear distortion ω of the unit cell. The presence of this shear indicates that the crystal structure is not tetragonal but could be for instance orthorhombic or monoclinic (see discussion in Supplementary Information 3). The orthorhombic cell can be described as pseudo-monoclinic with polarization vectors along the <011> directions. The direction of the horizontal component of the polarization vector (left or right) is related to the sign of the shearing angle, which alternates between negative and positive values ($+\omega$ or $-\omega$) along the growth direction. The polarization vectors projected in the image plane can point for example down-left/down-right in the horizontal stripes located in the bottom domain (shown in blue in Fig. 4(h)) and up-left/up-right in the stripes located in the triangular domains at the top (displayed in yellow). Stripes that show the same contrast in horizontal dark-field images have the same horizontal polarization component but the vertical component can differ. There are at least four variants of polarization and there might be more than four if the polarization vectors have an additional component along the electron beam direction, but this can hardly be determined experimentally. Each 180° domain is populated with at least two variants of polarization but the average polarization over the total area of a 180° domain should be vertical, either up or down. The 180° domains can be considered as *superdomains* similarly to 180° *superdomains* composed of tetragonal stripes, which were previously described in single crystals of $BaTiO_3$ [55]. Finally, the horizontal stripes are not present everywhere in the film, which indicates that this sheared phase coexists with the usual tetragonal phase with out-of-plane *c*-axis.

3.3. Ferroelectric domain switching using in-situ *biasing*

In-situ biasing was carried out in TEM to understand the influence of external electric fields on the 180° domains and the horizontal stripes. Again, observations were carried out using dark-field imaging and the experiment was conducted twice using vertical $(220)_{ortho}$ dark-field and subsequently horizontal $(004)_{ortho}$ dark-field. Fig. 5(a) is a low magnification image that shows the $NdScO_3/BaTiO_3/Pt$ stack and the conductive (B-doped) diamond probe. The probe was placed in direct contact with the Pt capping layer and care was taken so that the probe does not apply a significant mechanical stress to the sample. Fig. 5(b) is a schematic of the electrical setup. A bias voltage was applied between the top Pt electrode and the supporting Cu grid, which was located below the substrate in this experiment, to produce an electric field that is primarily vertical in the $BaTiO_3$ layer.

3.3.1. Vertical polarization contrast (180° domains)

Fig. 5(c) is a series of vertical $(\text{-2-20})_{ortho}$ dark-field images that shows the evolution of the 180° domains in the presence of different applied electric fields. Images were extracted from the video 1 provided in Supplementary Materials. The voltage was increased progressively with regular steps of 12 V. In the initial situation (at 0 V), small triangular-shaped domains are visible in the top part of the layer with a darker contrast compared to the rest of the layer. The dark-field contrast is inverted with respect to Fig. 3(b-d) because the opposite diffraction

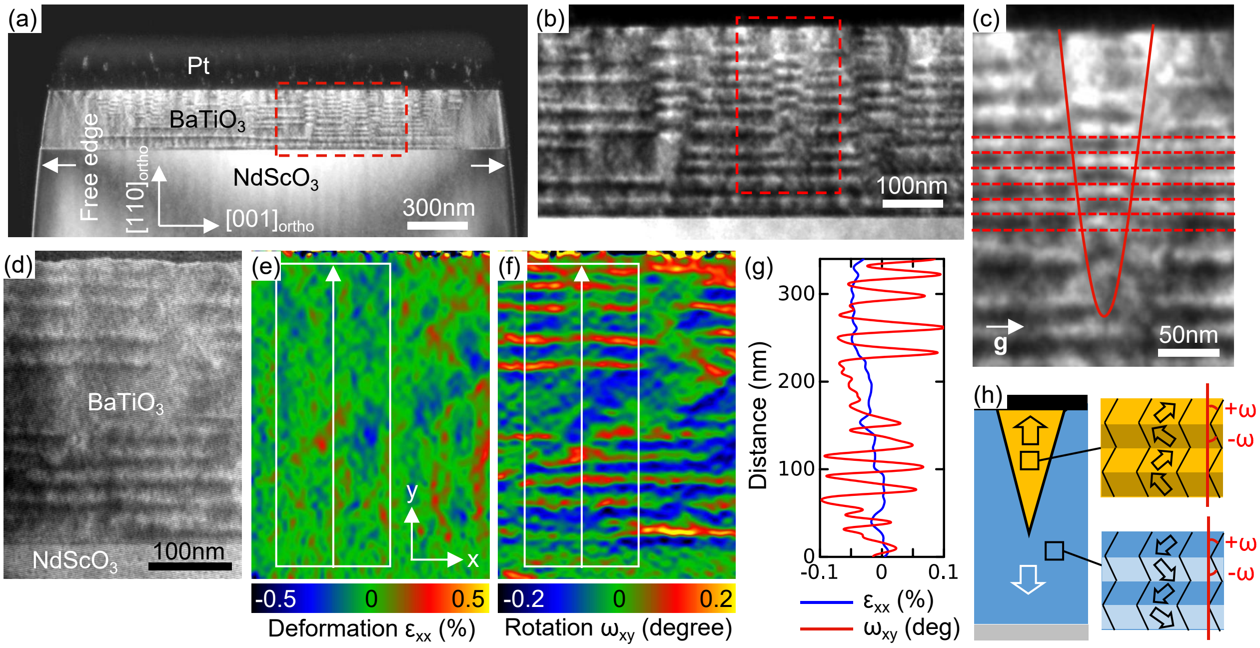

Figure 4. (a) Horizontal $(004)_{\mathrm{ortho}}$ dark-field TEM image of a lamella cut parallel to the $[001]_{\mathrm{ortho}}$ direction. Additional cuts were made on the left and right sides of the lamella as indicated by arrows. (b) Magnified image of the region indicated by a dashed rectangle in (a). (c) Magnified image of the top region of the layer as indicated by a dashed rectangle in (b). Red solid curve indicates a 180° domain wall and horizontal dashed red lines indicate stripe domain walls. (d) $(004)_{\mathrm{ortho}}$ dark-field electron hologram. (e,f) Corresponding ε_{xx} deformation and ω_{xy} rotation maps reconstructed from the hologram using Fourier transforms. (g) Deformation and rotation profiles extracted from the images in (e,f) along the vertical arrows and averaged horizontally according to the rectangles. (h) Corresponding schematic of the ferroelectric domain structure where $+\omega$ and $-\omega$ denote the shear angle of the crystalline structure. Angles have been exaggerated on purpose.

spot was selected ((-2-20) instead of (220)) with the objective aperture. The distribution and the shape of the 180° domains is also slightly different compared to the domains observed in Fig. 3(b-d). Here, the distribution of the domains is not continuous along the top interface as it shows gaps between them and their shape is narrower in the horizontal direction. These differences can be related to the fact that the top and bottom electrodes are not connected to the electrically grounded Cu grid as in Fig. 3. If interfacial charges are not compensated then the depolarization fields favor the alternation of antiparallel domains (oriented up and down) along the interface. The application of positive voltages (+12 V and +24 V) leads to the progressive growth of the dark domains towards the bottom interface. During the vertical growth, the domains maintain a tapered shape to reduce the density of charges at the domain wall. Once the apex of the domains has reached the bottom interface, they

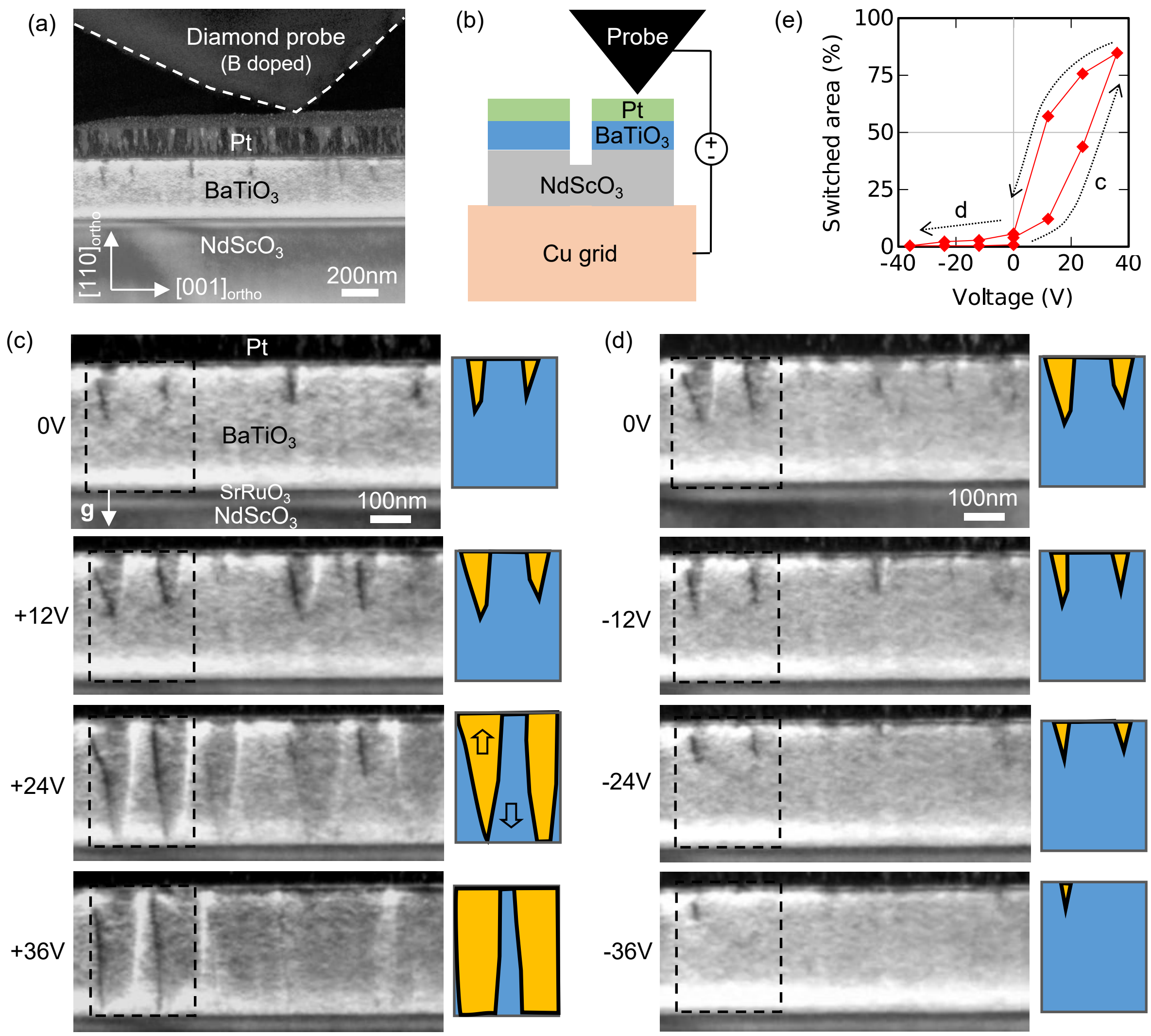

Figure 5. (a) Overview dark-field image of a lamella cut parallel to the $[001]_{ortho}$ direction and the probe (indicated by a dashed line) used to apply an electric field. (b) Corresponding schematic of the electrical setup. DC voltages were applied between the Pt top electrode and the supporting Cu grid at the bottom. (c) Series of $(\text{-2-20})_{ortho}$ dark-field images showing the motion of the 180° domains when applying different positive voltages indicated in the figure. Images were extracted from the video 1 provided in Supplementary Materials. Schematics on the right side represent the domain structures in the regions indicated by dashed rectangles. (d) Series of dark-field images obtained when applying different negative voltages indicated in the figure. (e) Hysteresis curve that shows the evolution of the area occupied by the darker domains (in percentage) with respect to the area occupied by the whole $BaTiO_3$ layer in the images as a function of the applied voltage.

start to expand horizontally until adjacent domains merge together (+36 V). During this horizontal expansion, the domain walls are oriented nearly perpendicular to the interfaces, to remain charge neutral. When the voltage is decreased (see Supplementary video 1), the domain walls move in the opposite way, first horizontally, then vertically towards the top electrode. When applying negative voltages, as shown in Fig. 5(d), the triangular domains shrink progressively towards the top electrode until they are almost completely erased at -36 V. Fig. 5(e) is an hysteresis loop which was plotted by measuring the area occupied by the darker domains with respect to the total area occupied by the layer in the image. The curve shows a bias (horizontal shift) towards positive voltages, which is related to the preferential location of the domains near the top interface at zero-field. It shows also a vertical shift because the electric field used was not large enough to fully saturate the layer at positive voltages.

3.3.2. Horizontal polarization contrast (stripe domains)

Fig. 6(a) is a series of horizontal $(004)_{\mathrm{ortho}}$ dark-field images showing the evolution of the horizontal stripe domains when different positive voltages are applied. Images were extracted from the video 2 provided in Supplementary Materials. In the initial situation (see image at 0 V), the stripe domains seem to be disorganized as the layer shows different small groups of stripes, in particular in the top part of the layer where the triangular-shaped 180° domains are located. When the voltage is increased (+20 V and +30 V), a reorganization of the stripes occurs as the 180° domain walls move across the layer to reach the bottom electrode. At the largest voltage (+40 V), the layer exhibits long and regularly spaced horizontal stripes, which indicates that the 180° domains have reached a nearly *saturated* configuration. When the voltage is decreased back to zero (see top image in Fig. 6(b)), the 180° domain walls reappear in the layer and the stripe domains are again disorganized. The application of negative voltages lead to a qualitatively similar behavior, with an initially disordered state consisting of small groups of stripes, which turns progressively into to a well ordered state with long stripes (at -30 V). This new organized state is reached at a lower voltage compared to the positive series in (a) because of the bias of the hysteresis curve described in the previous section. The two saturated states obtained with positive and negative voltages (+40 V and -30 V) show a similar density of stripes (approximately 9 black/white repetitions can be counted through the thickness of the layer).

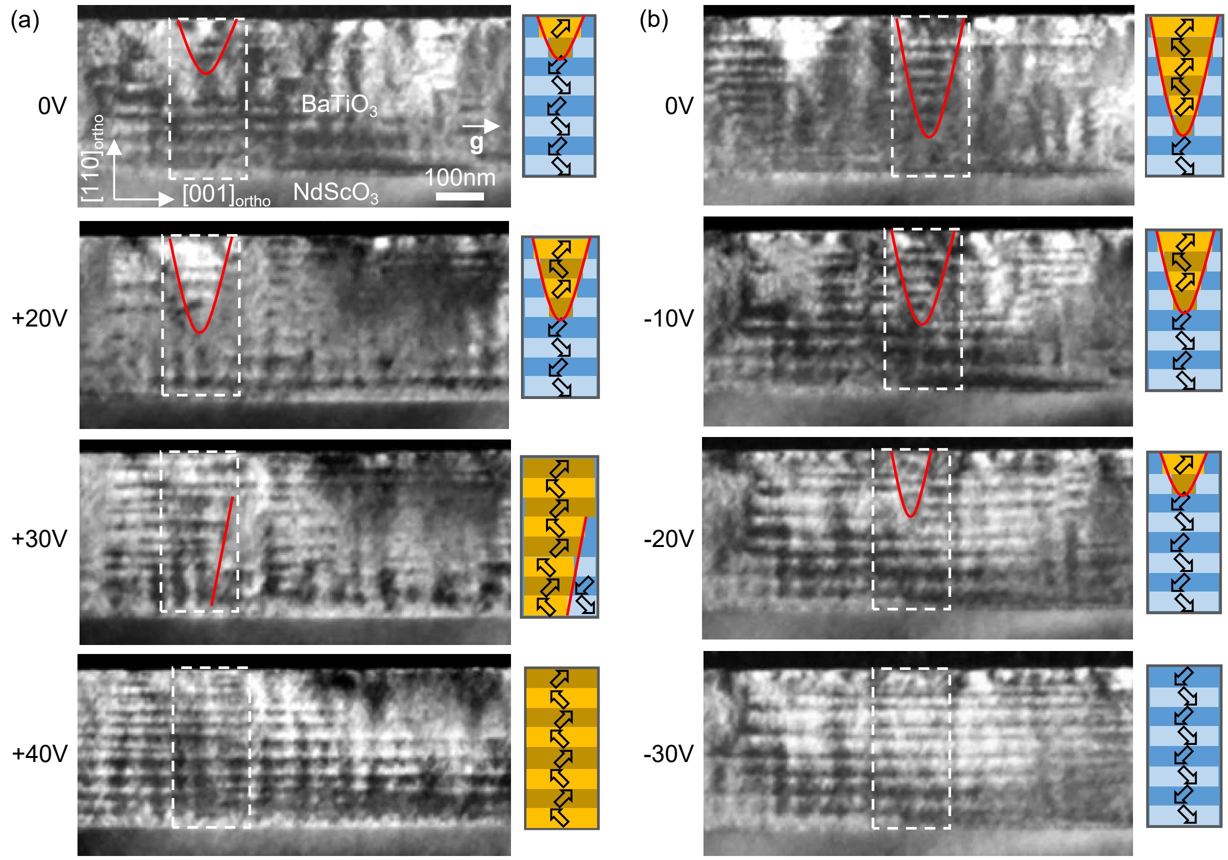

Figure 6. Series of $(004)_{ortho}$ dark-field images acquired while applying different (a) positive and (b) negative voltages indicated in the figure. Images were extracted from the video 2 provided in Supplementary Materials. Red curves indicate the position of a 180° domain wall. Schematics on the right side illustrate the domain structure in the regions indicated by dashed rectangles.

4. Discussion

We have investigated in TEM a 320 nm thick $BaTiO_3$ layer grown onto a $NdScO_3$ substrate with a 7 nm thick $SrRuO_3$ bottom electrode and a Pt capping electrode. The orthorhombic structure of $NdScO_3$ leads to anisotropic epitaxial strains. In the as-grown state, the $BaTiO_3$ layer shows anisotropic a/c ferroelastic domains that form gradually along the growth direction, and purely ferroelectric triangular-shaped 180° domains located in the top part of the film. This domain pattern can be modified in different ways depending on the orientation and the thickness of the TEM lamella. If the lamella is cut parallel to the largest strain direction (parallel to the $[1\text{-}10]_{ortho}$ direction), the a/c ferroelastic domain pattern is preserved. However, if the lamella is cut perpendicular to the largest strain direction (parallel to the $[001]_{ortho}$ direction), the layer shows thin horizontal stripe domains whose density increases when the edges of the lamella are released. These horizontal stripes exhibit a sheared crystalline structure with inclined polarization vectors and with at least four variants of polarization. Each 180° domain is populated with at least two variants and can be considered as a *superdomain* where the average polarization is vertical, either up or down. The shape and distribution of the 180° domains in the layer depends on the thickness of the lamella, the thickness of the top electrode and the connection of the electrodes to the ground.

The formation of bundles of ferroelastic stripe domains is a phenomenon frequently observed in thin slabs of $BaTiO_3$ single crystals [27, 56, 57]. It was suggested in a previous study that such stripe domains minimize stresses related to surface tension at the free edges of the lamella [58]. It was also shown that ≈ 10 nm thick damaged surface layers induced by implantation of gallium ions during FIB thinning do not have a significant influence on ferroelastic domains. The domain structure remains nearly the same after thermal annealing to repair damaged surfaces [58]. However, in previously cited studies, the stripe domains were tetragonal a/c twins, which do not correspond with the sheared domains observed here. This can be explained by the special boundary conditions provided by the substrate and the geometry of the lamella. In the bulk state, the anisotropic a/c domains form to relax the interfacial strain of -0.45% along the [1-10] direction. This boundary condition is partly released when creating a thin lamella perpendicular to this direction. The release can be significant because of the aspect ratio since the lamella is thinner than the layer (approximately 100 nm thick and 320 nm thick respectively). In addition, new electrostatic boundary conditions appear at the free surfaces of the lamella, which are not favorable to this a/c pattern as the polarization in the a domains would point directly towards the free surfaces and induce depolarization fields. The formation of new domains with polarization vectors oriented in the plane of the lamella is more favorable and their ferroelastic structure is then influenced by the weak remaining strain of -0.05% along the $[001]_{\mathrm{ortho}}$ direction. This strain is probably too small to induce a/c domains in this direction and the layer prefers to balance it by forming horizontal stripes where the structure and the polarization show an inclination alternating between the left and right directions. The density of stripes increases when additional cuts are made on the sides of the lamella, which also show that free edges play an important role in the formation of the stripes. These domains could possibly be 90° orthorhombic (or monoclinic) twins whose polar vectors are inclined with respect to the interfaces. In bulk $BaTiO_3$, the tetragonal-to-orthorhombic phase transition occurs quite close to room temperature (5°C to 15°C) [59]. In addition, previous investigations of lamellas cut parallel to the $[1\text{-}10]_{\text{ortho}}$ direction have shown that the layer exhibits an orthorhombic symmetry close to the bottom interface [40].

In the presence of an external electric field, the 180° domain walls move vertically and maintain a tapered triangular shape to minimize charges. Once they have reached the bottom interface, they move laterally until adjacent domains merge. The movements of the 180° domain walls do not seem to be influenced by the ferroelastic stripe domains. Unlike tetragonal twins, which can slow down and influence the growth of 180° domains [22, 23], the horizontal stripes are able to quickly redistribute themselves as the 180° domain walls move through the layer. Nearly perfect bundles of horizontal stripes are obtained when a large voltage is applied so that the 180° domain structure is saturated either up or down. 180° domains were found to be also sensitive to electric fields generated at the edges of the TEM illumination (see Supplementary Information 4). They can be switched by shifting the illumination on the specimen and therefore care should be taken when focusing and shifting the beam.

5. Conclusion

Ferroelectric domains in a low-strain $BaTiO_3$ thin film grown onto $NdScO_3$ substrate were investigated using transmission electron microscopy. It was observed that the purely ferroelectric domain structure, consisting of triangular-shaped 180° domains, is sensitive the thickness of the lamellas and the grounding of the electrodes. The ferroelastic domain structure, consisting of a/c tetragonal twins, is sensitive to the thinning direction. When the lamella is cut perpendicular to the largest strain direction, the a/c twins are replaced by thin stripes parallel to the interfaces. These stripes have a sheared structure and can form bundles that populate the 180° domains. In the presence of external electric fields, these 180° *superdomains* grow along the vertical direction and subsequently the horizontal direction. The motion of 180° domain walls is not hindered by the horizontal stripe domains, which can quickly redistribute themselves. These different observations show that the geometry and the boundary conditions in a TEM lamella have the ability to alter the ferroelastic and ferroelectric domain structure of an epitaxial thin film.

Acknowledgments

T.D. acknowledges the European Metrology Research Programme (EMRP) project IND54 (Nanostrain). A.S.E. acknowledges financial support from the alumni organization of the University of Groningen, De-Aduarderking (Ubbo Emmius Fonds), and from the Zernike Institute for Advanced Materials. M. Legros is acknowledged for helping with the Hysitron holder. B. Noheda is acknowledged for commenting on the manuscript.

References

[1] M. Dawber, K. M. Rabe, and J. F. Scott. Physics of thin-film ferroelectric oxides. *Reviews of Modern Physics*, 77:1083–1130, Oct 2005.

[2] P. Muralt. Recent progress in materials issues for piezoelectric MEMS. *Journal of the American Ceramic Society*, 91(5):1385–1396, 2008.

[3] S. K. Streiffer, J. A. Eastman, D. D. Fong, C. Thompson, A. Munkholm, M. V. Ramana Murty, O. Auciello, G. R. Bai, and G. B. Stephenson. Observation of nanoscale 180° stripe domains in ferroelectric $PbTiO_3$ thin films. *Physical Review Letters*, 89:067601, Jul 2002.

[4] D. D. Fong, G. B. Stephenson, S. K. Streiffer, J. A. Eastman, O. Auciello, P. H. Fuoss, and C. Thompson. Ferroelectricity in ultrathin perovskite films. *Science*, 304(5677):1650–1653, 2004.

[5] C. Thompson, D. D. Fong, R. V. Wang, F. Jiang, S. K. Streiffer, K. Latifi, J. A. Eastman, P. H. Fuoss, and G. B. Stephenson. Imaging and alignment of nanoscale 180° stripe domains in ferroelectric thin films. *Applied Physics Letters*, 93(18):182901, 2008.

[6] B. S. Kwak, A. Erbil, J. D. Budai, M. F. Chisholm, L. A. Boatner, and B. J. Wilkens. Domain formation and strain relaxation in epitaxial ferroelectric heterostructures. *Physical Review B*, 49:14865–14879, Jun 1994.

[7] C. S. Ganpule, V. Nagarajan, H. Li, A. S. Ogale, D. E. Steinhauer, S. Aggarwal, E. Williams, R. Ramesh, and P. De Wolf. Role of 90° domains in lead zirconate titanate thin films. *Applied Physics Letters*, 77(2):292–294, 2000.

[8] I. Vrejoiu, G. Le Rhun, N. D. Zakharov, D. Hesse, L. Pintilie, and M. Alexe. Threading

dislocations in epitaxial ferroelectric $PbZr_{0.2}Ti_{0.8}O_3$ films and their effect on polarization backswitching. *Philosophical Magazine*, 86(28):4477–4486, 2006.

[9] A. L. Roitburd. Equilibrium structure of epitaxial layers. *physica status solidi (a)*, 37(1):329–339, 1976.

[10] W. Pompe, X. Gong, Z. Suo, and J. S. Speck. Elastic energy release due to domain formation in the strained epitaxy of ferroelectric and ferroelastic films. *Journal of Applied Physics*, 74(10):6012–6019, 1993.

[11] D. G. Schlom, L.-Q. Chen, C.-B. Eom, K. M. Rabe, S. K. Streiffer, and J.-M. Triscone. Strain tuning of ferroelectric thin films. *Annual Review of Materials Research*, 37(1):589–626, 2007.

[12] A. R. Damodaran, J. C. Agar, S. Pandya, Z. Chen, L. Dedon, R. Xu, B. Apgar, S. Saremi, and L. W. Martin. New modalities of strain-control of ferroelectric thin films. *Journal of Physics: Condensed Matter*, 28(26):263001, May 2016.

[13] G. F. Nataf and M. Guennou. Optical studies of ferroelectric and ferroelastic domain walls. *Journal of Physics: Condensed Matter*, 32(18):183001, February 2020.

[14] G. Y. Robinson and R. M. White. Scanning electron microscopy of ferroelectric domains in barium titanate. *Applied Physics Letters*, 10(11):320–323, 1967.

[15] K. A. Hunnestad, E. D. Roede, A. T. J. van Helvoort, and D. Meier. Characterization of ferroelectric domain walls by scanning electron microscopy. *Journal of Applied Physics*, 128(19):191102, 2020.

[16] A. Gruverman and S. V. Kalinin. Piezoresponse force microscopy and recent advances in nanoscale studies of ferroelectrics. *Journal of Materials Science*, 41(1):107–116, 2006.

[17] E. Soergel. Piezoresponse force microscopy (PFM). *Journal of Physics D: Applied Physics*, 44(46):464003, November 2011.

[18] P. Zubko, N. Stucki, C. Lichtensteiger, and J.-M. Triscone. X-ray diffraction studies of 180° ferroelectric domains in $PbTiO_3/SrTiO_3$ superlattices under an applied electric field. *Physical Review Letters*, 104:187601, May 2010.

[19] C. L. Jia, M. Lentzen, and K. Urban. Atomic-resolution imaging of oxygen in perovskite ceramics. *Science*, 299(5608):870–873, 2003.

[20] C.-L. Jia, V. Nagarajan, J.-Q. He, L. Houben, T. Zhao, R. Ramesh, K. Urban, and R. Waser. Unit-cell scale mapping of ferroelectricity and tetragonality in epitaxial ultrathin ferroelectric films. *Nature Materials*, 6(1):64–69, January 2007.

[21] C. T. Nelson, B. Winchester, Y. Zhang, S.-J. Kim, A. Melville, C. Adamo, C. M. Folkman, S.-H. Baek, C.-B. Eom, D. G. Schlom, L.-Q. Chen, and X. Pan. Spontaneous vortex nanodomain arrays at ferroelectric heterointerfaces. *Nano Letters*, 11(2):828–834, 2011.

[22] P. Gao, J. Britson, J. R. Jokisaari, C. T. Nelson, S.-H. Baek, Y. Wang, C.-B. Eom, L.-Q. Chen, and X. Pan. Atomic-scale mechanisms of ferroelastic domain-wall-mediated ferroelectric switching. *Nature Communications*, 4:–, November 2013.

[23] J. K. Lee, G. Y. Shin, K. Song, W. S. Choi, Y. A. Shin, S. Y. Park, J. Britson, Y. Cao, L.-Q. Chen, H. N. Lee, and S. H. Oh. Direct observation of asymmetric domain wall motion in a ferroelectric capacitor. *Acta Materialia*, 61(18):6765–6777, 2013.

[24] L. Li, L. Xie, and X. Pan. Real-time studies of ferroelectric domain switching: a review. *Reports on Progress in Physics*, 82(12):126502, November 2019.

[25] J. M. Gibson, R. Hull, J. C. Bean, and M. M. J. Treacy. Elastic relaxation in transmission electron microscopy of strained-layer superlattices. *Applied Physics Letters*, 46(7):649–651, 1985.

[26] M. M. J. Treacy and J. M. Gibson. The effects of elastic relaxation on transmission electron microscopy studies of thinned composition-modulated materials. *Journal of Vacuum Science & Technology B*, 4(6):1458–1466, 1986.

[27] A. Schilling, T. B. Adams, R. M. Bowman, J. M. Gregg, G. Catalan, and J. F. Scott. Scaling of domain periodicity with thickness measured in $BaTiO_3$ single crystal lamellae and comparison with other ferroics. *Physical Review B*, 74:024115, Jul 2006.

[28] C. Kittel. Theory of the structure of ferromagnetic domains in films and small particles. *Physical Review*, 70:965–971, Dec 1946.

[29] T. Mitsui and J. Furuichi. Domain structure of rochelle salt and KH_2PO_4. *Physical Review*, 90:193–202, Apr 1953.

[30] A. Schilling, R. M. Bowman, G. Catalan, J. F. Scott, and J. M. Gregg. Morphological control of polar orientation in single-crystal ferroelectric nanowires. *Nano Letters*, 7(12):3787–3791, December 2007.

[31] G. Catalan, A. Schilling, J. F. Scott, and J. M. Gregg. Domains in three-dimensional ferroelectric nanostructures: theory and experiment. *Journal of Physics: Condensed Matter*, 19(13):132201, 2007.

[32] A. Schilling, D. Byrne, G. Catalan, K. G. Webber, Y. A. Genenko, G. S. Wu, J. F. Scott, and J. M. Gregg. Domains in ferroelectric nanodots. *Nano Letters*, 9(9):3359–3364, 2009.

[33] T. Matsumoto and M. Okamoto. Effects of electron irradiation on the ferroelectric 180° in-plane nanostripe domain structure in a thin film prepared from a bulk single crystal of $BaTiO_3$ by focused ion beam. *Journal of Applied Physics*, 109(1):014104, 2011.

[34] R. Ahluwalia, N. Ng, A. Schilling, R. G. P. McQuaid, D. M. Evans, J. M. Gregg, D. J. Srolovitz, and J. F. Scott. Manipulating ferroelectric domains in nanostructures under electron beams. *Physical Review Letters*, 111:165702, Oct 2013.

[35] J. L. Hart, S. Liu, A. C. Lang, A. Hubert, A. Zukauskas, C. Canalias, R. Beanland, A. M. Rappe, M. Arredondo, and M. L. Taheri. Electron-beam-induced ferroelectric domain behavior in the transmission electron microscope: Toward deterministic domain patterning. *Physical Review B*, 94:174104, Nov 2016.

[36] Z. Chen, X. Wang, S. P. Ringer, and X. Liao. Manipulation of nanoscale domain switching using an electron beam with omnidirectional electric field distribution. *Physical Review Letters*, 117:027601, Jul 2016.

[37] V. G. Koukhar, N. A. Pertsev, and R. Waser. Thermodynamic theory of epitaxial ferroelectric thin films with dense domain structures. *Physical Review B*, 64:214103, Nov 2001.

[38] A. Grünebohm, M. Marathe, and C. Ederer. Ab initio phase diagram of $BaTiO_3$ under epitaxial strain revisited. *Applied Physics Letters*, 107(10):102901, 2015.

[39] A. S. Everhardt, S. Matzen, N. Domingo, G. Catalan, and B. Noheda. Ferroelectric domain structures in low-strain $BaTiO_3$. *Advanced Electronic Materials*, 2(1):1500214, 2016.

[40] A. S. Everhardt, T. Denneulin, A. Grünebohm, Y.-T. Shao, P. Ondrejkovic, S. Zhou, N. Domingo, G. Catalan, J. Hlinka, J.-M. Zuo, S. Matzen, and B. Noheda. Temperature-independent giant dielectric response in transitional $BaTiO_3$ thin films. *Applied Physics Reviews*, 7(1):011402, 2020.

[41] F. Fujimoto. Dynamical theory of electron diffraction in Laue-case, i. general theory. *Journal of the Physical Society of Japan*, 14(11):1558–1568, 1959.

[42] M. Tanaka and G. Honjo. Electron optical studies of barium titanate single crystal films. *Journal of the Physical Society of Japan*, 19(6):954–970, 1964.

[43] T. Asada and Y. Koyama. Coexistence of ferroelectricity and antiferroelectricity in lead zirconate titanate. *Physical Review B*, 70:104105, Sep 2004.

[44] T. Asada and Y. Koyama. Ferroelectric domain structures around the morphotropic phase boundary of the piezoelectric material $PbZr_{1-x}Ti_xO_3$. *Physical Review B*, 75:214111, Jun 2007.

[45] K. Aoyagi, T. Kiguchi, Y. Ehara, T. Yamada, H. Funakubo, and T. J. Konno. Diffraction contrast analysis of 90° and 180° ferroelectric domain structures of $PbTiO_3$ thin films. *Science and Technology of Advanced Materials*, 12(3):034403, 2011.

[46] M. Hÿtch, F. Houdellier, F. Hüe, and E. Snoeck. Nanoscale holographic interferometry for strain measurements in electronic devices. *Nature*, 453(7198):1086–1089, 2008.

[47] T. Denneulin, N. Wollschläger, A. S. Everhardt, S. Farokhipoor, B. Noheda, E. Snoeck, and M. Hÿtch. Local deformation gradients in epitaxial $Pb(Zr_{0.2}Ti_{0.8})O_3$ layers investigated by transmission electron microscopy. *Journal of Physics: Condensed Matter*, 30(21):215701, April 2018.

[48] R. Uecker, B. Velickov, D. Klimm, R. Bertram, M. Bernhagen, M. Rabe, M. Albrecht, R. Fornari, and D. G. Schlom. Properties of rare-earth scandate single crystals (Re=Nd-Dy). *Journal of Crystal Growth*, 310(10):2649–2658, 2008.

[49] G. H. Kwei, A. C. Lawson, S. J. L. Billinge, and S. W. Cheong. Structures of the ferroelectric phases of barium titanate. *The Journal of Physical Chemistry*, 97(10):2368–2377, 1993.

[50] J. J. Wang, F. Y. Meng, X. Q. Ma, M. X. Xu, and L. Q. Chen. Lattice, elastic, polarization, and electrostrictive properties of $BaTiO_3$ from first-principles. *Journal of Applied Physics*, 108(3):034107, 2010.

[51] M. Y. Gureev, A. K. Tagantsev, and N. Setter. Head-to-head and tail-to-tail 180° domain walls in an isolated ferroelectric. *Physical Review B*, 83:184104, May 2011.

[52] R. M. Langford and A. K. Petford-Long. Preparation of transmission electron microscopy cross-section specimens using focused ion beam milling. *Journal of Vacuum Science & Technology A: Vacuum, Surfaces, and Films*, 19(5):2186–2193, 2001.

[53] J. F. Scott. Nanoferroelectrics: statics and dynamics. *Journal of Physics: Condensed Matter*, 18(17):R361–R386, April 2006.

[54] L. J. McGilly, L. Feigl, and N. Setter. Domain nucleation behavior in ferroelectric films

with thin and ultrathin top electrodes versus insulating top layers. *Thin Solid Films*, 636:214–219, 2017.

[55] L. J. McGilly and J. M. Gregg. Scaling of superdomain bands in ferroelectric dots. *Applied Physics Letters*, 98(13):132902, 2011.

[56] L. J. McGilly, A. Schilling, and J. M. Gregg. Domain bundle boundaries in single crystal $BaTiO_3$ lamellae: Searching for naturally forming dipole flux-closure/quadrupole chains. *Nano Letters*, 10(10):4200–4205, 2010.

[57] R. G. P. McQuaid, L. J. McGilly, P. Sharma, A. Gruverman, and J. M. Gregg. Mesoscale flux-closure domain formation in single-crystal $BaTiO_3$. *Nature Communications*, 2:404, July 2011.

[58] I. A. Luk'yanchuk, A. Schilling, J. M. Gregg, G. Catalan, and J. F. Scott. Origin of ferroelastic domains in free-standing single-crystal ferroelectric films. *Physical Review B*, 79:144111, Apr 2009.

[59] T. Limboeck and E. Soergel. Evolution of ferroelectric domain patterns in $BaTiO_3$ at the orthorhombic - tetragonal phase transition. *Applied Physics Letters*, 105(15):152901, 2014.